DOI: 10.1002/ejic.200800805

Rate-Redox-Controlled Size-Selective Synthesis of Silver Nanoparticles Using Polyoxometalates

Aristidis Troupis,*[a] Theodoros Triantis,[a] Anastasia Hiskia,[a] and Elias Papaconstantinou*[a]

Keywords: Polyoxometalates / Nanostructures / Silver nanoparticles / Rate-redox-controlled reactions

Uniform silver nanoparticles were obtained upon the reduction of silver ions by reduced polyoxometalates (POMs) by simple mixing at room temperature. Control of the size and the dispersity of silver nanoparticles was achieved by rate control. Faster reduction of Ag^+ led to smaller and more uniform silver nanoparticles, suggesting that the rate of Ag^+ reduction strongly affects the initial nucleation of silver particles. A faster rate is achieved by either (i) increasing the concentration of the reducing reagent (reduced POM) or, more interestingly (ii) selecting POMs having appropriate (more negative) redox potentials: different POMs with increasing negative reduction potential or the same POM with more electrons accumulated on it. The rates of Ag^+ reduction parallel the more negative reduction potential for POMs according to the series $H_2W_{12}O_{40}^{7-} > SiW_{12}O_{40}^{5-} > P_2W_{18}O_{62}^{8-} > P_2W_{18}O_{62}^{7-} > P_2Mo_{18}O_{62}^{10-} > P_2Mo_{18}O_{62}^{8-} = 0$. This precise redox-control is summarized in a $\log k$ (E_0) electrochemical-like behavior, in alliance to a "soluble cathode" behavior of POMs, which leads to more uniform particles than those obtained with conventional electrochemistry. Alternatively, the concentration of silver ions influences the size of the particles obtained: increasing the amount of Ag^+ leads to larger nanoparticles.

Introduction

Colloidal sols of metal nanoparticles are of intriguing interest because of their fascinating photochemical, photovoltaic, and optoelectronic properties,[1] as well as their catalytic role in various chemical reactions.[2] Since these properties are a function of the size of the dispersed metal particles, the establishment of methods by which we could control and select the size of the particles produced is of paramount interest in order to maximize the efficiency of the particles[3] and remains an issue of tremendous importance in nanochemistry.

POMs are precisely defined anionic metal oxides that have dynamically entered the realm of the synthesis of metal nanoparticles, presented as both *catalytic reducing* reagents and stabilizers for the synthesis of Ag, Au, Pd, and Pt nanoparticles of reasonably good dispersity, upon illumination with UV/near-Vis light.[4] In the process, POMs absorb UV light and abstract electrons from oxidizable organic substrates, S, in this case alcohols.[5]

$$POM + S \xrightarrow{h\nu} POM(e\text{-}) + S_{ox} \quad (1)$$

Then, in their reduced form, POMs reduce metal ions to the corresponding metal nanoparticles, via, for example, Equation (2).

$$POM(e\text{-}) + Ag^+ \rightarrow POM + Ag^0_{colloidal} \quad (2)$$

This photocatalytic process has been the basis for the preparation by Sastry and co-workers of more complicated nanostructures such as Au–Ag core-shell dimetallic compounds, Au nanosheets and Ag nanorings.[6] Ershov and Gordeev presented the ability of POMs to act as catalytic reducing reagents and stabilizers upon radiolysis of aqueous solutions of metal ions for the formation of Ag, Cu, Cd, Tl, Pd, Co, and Ni nanoparticles.[7] Recently, Shen et al. have shown that by varying operational parameters such as the ratio $[Ag^+]/[POM]$, the pH, or the temperature of reaction, the size and shape of the silver nanoparticles obtained can be controlled, which leads to Ag nanorods as well.[8a]

Herein, by isolating and examining reaction (2), we show that size selectivity can be achieved on the basis of rate control. Not only by increasing the concentration of the reductant (reduced POM) but, more interestingly, by tuning its redox potential, can we control the rate of Ag^+ reduction and consequently the size of the formed nanoparticles. The unique ability of POMs to exhibit widely varied and precisely controlled redox potentials depending on intrinsic

[a] NCSR Demokritos, Institute of Physical Chemistry, 73 Neapoleos, 15310 Agia Paraskevi, Attiki, Greece
Fax: +30-210-6511766
E-mail: epapac@chem.demokritos.gr

Supporting information for this article is available on the WWW under http://www.eurjic.org/ or from the author.

properties provides an advanced tool.[8b] For this reason, we have used a variety of POMs selected from the two classical types of Keggin and Dawson structures (Figure 1).

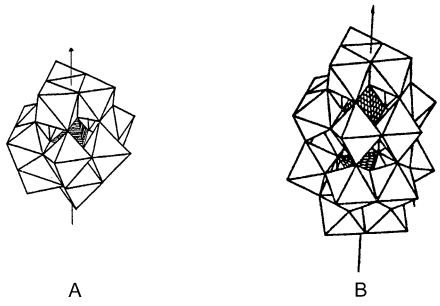

Figure 1. Characteristic structures of POMs. (A) The $XM_{12}O_{40}^{n-}$, Keggin structure is composed of MO_6 octahedra sharing corners and edges. The heteroatom X = P, Si, or H_2 is within the central (shaded) tetrahedron XO_4. (B) The $P_2M_{18}O_{62}^{6-}$, Wells-Dawson structure, comes from the Keggin ion by removing three MO_6 octahedra and joining the two 9-metalo half units (M = Mo or W).

In particular, the following reduced POMs, herein produced photochemically, were tested in the reduction of Ag^+ to Ag^0 nanoparticles: the one-electron-reduced Keggin POMs $SiW_{12}O_{40}^{4-}$ and $H_2W_{12}O_{40}^{6-}$ ($SiW_{12}O_{40}^{5-}$ and $H_2W_{12}O_{40}^{7-}$), the one-electron- and two-electron-reduced Dawson phosphotungstate $P_2W_{18}O_{62}^{6-}$ ($P_2W_{18}O_{62}^{7-}$ and $P_2W_{18}O_{62}^{8-}$), and the two-electron- and four-electron-reduced Dawson phosphomolybdate $P_2Mo_{18}O_{62}^{6-}$ ($P_2Mo_{18}O_{62}^{8-}$ and $P_2Mo_{18}O_{62}^{10-}$). These reagents exhibit a wide range of redox potentials depending on either the nature of POM or the extent of reduction in the same POM (Figure 2).

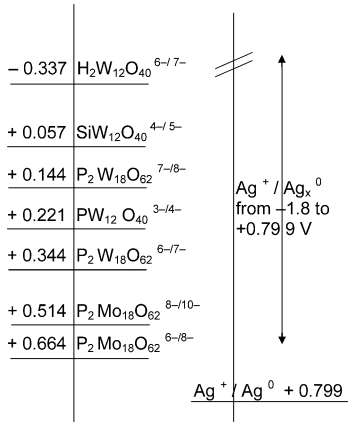

Figure 2. Redox potentials of POM anions and silver ions (V vs. NHE).

Results and Discussion

1. Formation of Ag^0 Nanoparticles: POMs as Stoichiometric, Single-Electron Relays for the Reduction of Ag^+

At first, in all cases, the reducing agent [reduced POM, POM(e-)] was produced photochemically by reaction (1). For instance, a deaerated $P_2W_{18}O_{62}^{6-}$/propan-2-ol solution illuminated with $\lambda > 320$ nm gradually turns blue due to photoreduction to $P_2W_{18}O_{62}^{7-}$. The concentration of the resulting reduced POM was monitored by visible absorption spectrometry by means of its characteristic peak at 714 nm. When the desired concentration was obtained, the cell was removed from the photolysis lamp.

In turn, in the absence of light, the POM(e-) solution obtained was mixed with a deaerated Ag^+ solution and agitated to obtain Ag^0 nanoparticles by reaction (2). The process was monitored by visible absorption spectrometry, by means of the characteristic absorbance peak for the one-electron-reduced POM, $P_2W_{18}O_{62}^{7-}$, at 714 nm (curve for 0 min in Figure 3). Upon mixing with Ag^+, a gradual decrease in the size of this peak was observed with the concomitant appearance of the plasmon resonance peak of colloidal silver at 420 nm (Figure 3). Within 40 min, when the formation of silver nanoparticles was completed, the initially blue color solution was converted to green and finally yellow. These observations indicate electron transfer from reduced POM to Ag^+ by reaction (3).

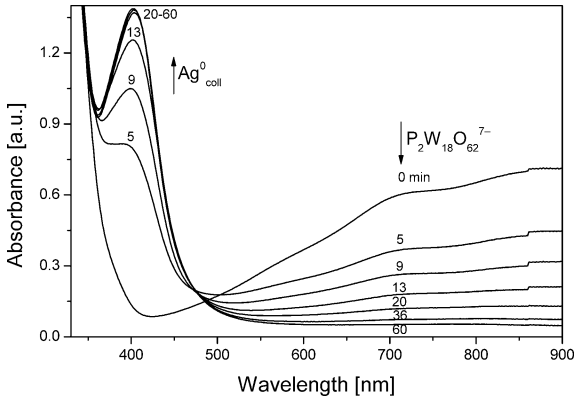

Figure 3. Absorption spectra showing the disappearance of the 1-equivalent-reduced POM $P_2W_{18}O_{62}^{7-}$ (peak at 714 nm) and the concomitant formation of silver nanoparticles (peak at 420 nm), upon mixing reduced POM $P_2W_{18}O_{62}^{7-}$ (2×10^{-4} M) [obtained by illumination of a deaerated solution $P_2W_{18}O_{62}^{6-}$ (2×10^{-4} M) and propan-2-ol (1.0 M)] with Ag^+ (10^{-4} M).

$$P_2W_{18}O_{62}^{7-} + Ag^+ \rightarrow P_2W_{18}O_{62}^{6-} + Ag^0_{coll} \quad (3)$$

Thus, reaction (2) is easily monitored. From the known absorption coefficient for the reduced POM (a tool that easily counts the excess electron charge on the reduced POM), one can derive the temporal profile for reaction (2), by taking also into account the absorption coefficient for colloidal silver (as it is calculated at the saturation point of the reaction when all silver has been reduced). Figure 4a depicts the decrease in concentration of $P_2W_{18}O_{62}^{7-}$ and the concomitant formation of silver nanoparticles with time and shows that the rate of consumption of the reducing reagent equals to the rate of formation of silver nanoparticles, verifying the 1:1 stoichiometry for reaction (3). Figure 4a also indicates that there is 100% conversion of Ag^+ to Ag^0. Please note that the process is photocatalytic and can go on provided that fresh POM, alcohol, and Ag^+ are added to the

solution. Similar results were also obtained in the case of other reducing reagents, the one-electron-reduced POMs $SiW_{12}O_{40}^{5-}$ and $H_2W_{12}O_{40}^{7-}$, which are also one-electron donors (see Figure 4b, c).[9]

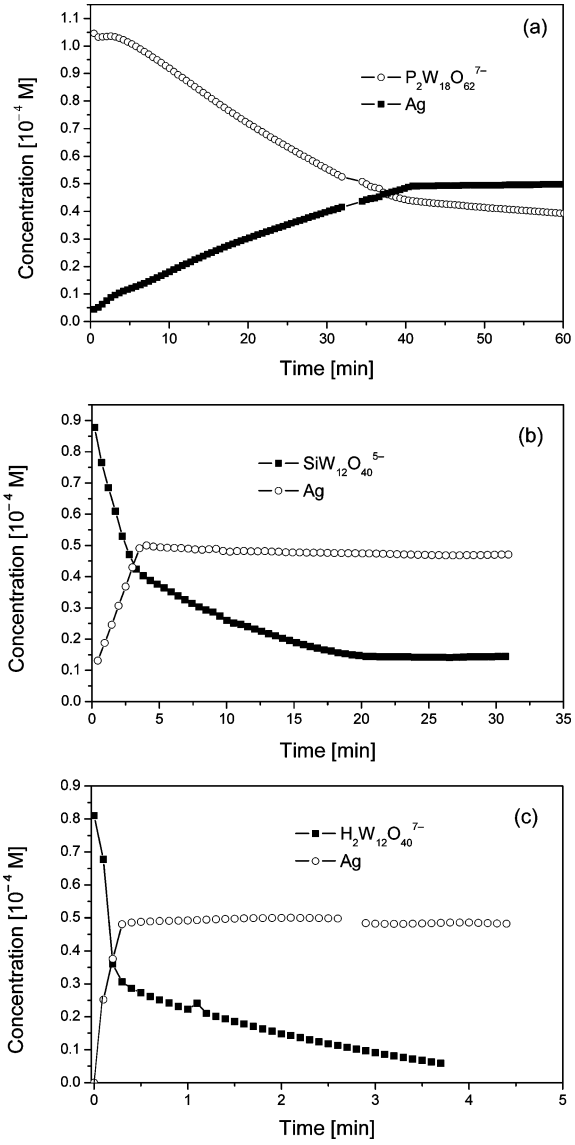

Figure 4. Decrease in POM(e-) concentration and formation of Ag^0 with reaction time for various POMs, (a) $P_2W_{18}O_{62}^{7-}$, (b) $SiW_{12}O_{40}^{5-}$, (c) $H_2W_{12}O_{40}^{7-}$, upon mixing reduced POM (1×10^{-4} M) [obtained by illumination of a deaerated solution POM (1×10^{-4} M) and propan-2-ol (1.0 M)] with Ag^+ (0.5×10^{-4} M).

The above discussion shows that the single-electron transfers triggered by reduced POMs can easily be monitored and controlled, and it would be interesting to examine whether this controllability can be converted to a control of the rate and subsequently the size and dispersity of the nanoparticles.

2. Rate- and Size-Controlled Synthesis of Silver Nanoparticles

By varying the concentration of reducing agent ($SiW_{12}O_{40}^{5-}$) from 1.0×10^{-4} M to 8.3×10^{-4} M, different rates and sizes are observed upon formation of Ag nanoparticles. In this set of experiments, the total concentration of POM (initial concentration of $SiW_{12}O_{40}^{4-}$) is kept constant (10^{-3} M) in order not to alter the stabilizing strength of the system (since POMs act as stabilizers as well). The initial concentration of Ag^+ is also kept constant (0.84×10^{-4} M). In all cases, $SiW_{12}O_{40}^{5-}$ is in excess in order to ensure that the same quantity, i.e. all, of Ag^+ is always reduced.

Increasing the concentration of reducing agent, $[SiW_{12}O_{40}^{5-}]_0$, results in a linear increase in the initial rate of reoxidation of $SiW_{12}O_{40}^{5-}$ to $SiW_{12}O_{40}^{4-}$ by Ag^+ ions (Figure 5, first-order dependence).

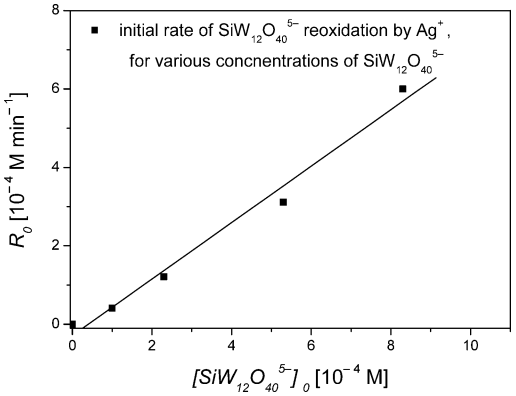

Figure 5. Effect of the initial concentration of $SiW_{12}O_{40}^{5-}$ on the initial rate of reoxidation of $SiW_{12}O_{40}^{5-}$ by Ag^+; reduced POM [obtained by illumination of a deaerated solution of $SiW_{12}O_{40}^{4-}$ (1.0 mM), and propan-2-ol (1.0 M)], Ag^+ (0.84 10^{-4} M). Values within 15%.

The TEM images of the corresponding silver nanoparticles are shown in Figure S1. Increasing the concentration of reducing agent results in the formation of gradually smaller nanoparticles (Table 1). For the lowest $[SiW_{12}O_{40}^{5-}]_0$, 1.0×10^{-4} M, the largest particles are obtained (beyond ca. 55 nm) with a wide distribution and more tailing in the size of the produced particles (Figure S1). The results based on TEM measurements are also in consistence with the visible absorption spectra of the corresponding nanoparticles (Figure S2), which exhibit a blue-shift with increasing $[SiW_{12}O_{40}^{5-}]_0$ (FigureS3), denoting a decrease in their size.[10]

Table 1. Average size of silver nanoparticles obtained upon reduction of Ag^+ (0.84×10^{-4} M) by various concentrations of $SiW_{12}O_{40}^{5-}$.

$[SiW_{12}O_{40}^{5-}]_0$ [M]	Diameter[a] [nm]	r.s.d.[b] [%]
8.3×10^{-4}	28.2	±19.0
5.3×10^{-4}	38.0	±21.4
2.3×10^{-4}	44.0	±10.6
1.0×10^{-4}	–	–

[a] Average diameter based on the counting of ca. 150 particles from the corresponding TEM images (Figure S1). [b] r.s.d.: relative standard deviation.

The fact that smaller Ag particles are formed with increasing rate of reduction implies that the nucleation process is enhanced more than the growth of silver nanoparticles. In this frame, at low rates of reduction, as is the case with the lowest concentration of reducing reagent, 0.1 mM, crystal growth might be important and leads to more dispersed and less spherical particles. In an analogous way, Finke has reported that, upon reduction of Ir^+ to Ir^0 nanoclusters by H_2 as reductant, more dispersed and less spherical iridium particles were obtained for the lowest hydrogen pressure.[11]

3. Redox-Controlled Synthesis of Silver Nanoparticles: POMs as "Soluble Nanocathodes"

Some intriguing and unique parameters in POM redox chemistry such as (i) their wide-ranged and precisely controlled redox potentials which may vary even in the same molecule by the accumulation of electrons (Figure 2), (ii) the unique ability of POMs to accept and release reversibly a large number of electrons one-by-one in a Coulomb staircase process, and (iii) their ability to trigger pure multielectron transfer reactions that are not accompanied by the formation or braking of bonds acting as multielectron relays in pure-electron transfer processes (as actually conventional electrodes do), have caused POMs to be regarded as soluble electrodes.[12] Herein we show their ability to release electrons controllably to Ag^+, acting as "soluble cathodes".

The rate of reaction (2) was measured while using various reducing reagents and by monitoring the disappearance of the absorbance peak at ca. 750 nm, characteristic for POM(e-). Figure 6 depicts that POMs with the more negative redox potentials are faster in electron transfer to Ag^+. The $\log k$ values for reaction (2)[13] parallel linearly the redox potentials of the corresponding POMs. This linearity of $\log k$ (E^0), which resembles the behavior of electrochemical circuits, combined with precise redox-tuning at distinct and wide-ranged reduction potentials, may render POMs "soluble nanocathodes" for the reduction of silver.

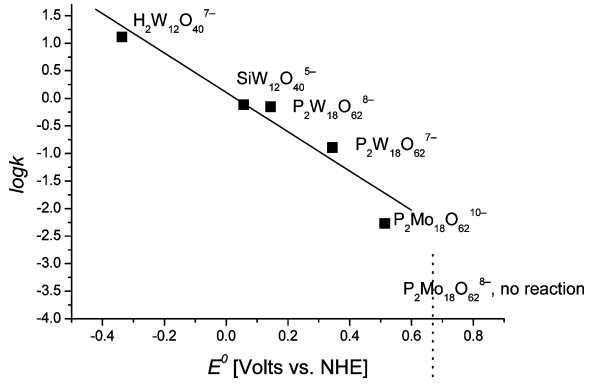

Figure 6. Linear function of $\log k$ vs. the reduction potential of various reduced POMs for the reduction of Ag^+ by various reduced POMs; reduced POM (1.0×10^{-4} M) [obtained by illumination of a deaerated solution POM (1.0×10^{-4} M) and propan-2-ol (1.0 M)], Ag^+ (0.5×10^{-4} M). Values within 15%.

3.1. Influence of the Kind of POM

More drastic changes to the rates and thus to size and dispersity of the particles (compared to the case of changing the concentration of reducing reagent) are observed by using different POMs. For instance, the influence of the kind of POM from the same series, the one-electron-reduced Keggin species $H_2W_{12}O_{40}^{7-}$ and $SiW_{12}O_{40}^{5-}$ is examined. The former, which exhibits a more negative redox potential [E^0 ($H_2W_{12}O_{40}^{6-}/H_2W_{12}O_{40}^{7-}$) = –0.337 V][5e,14] reacts ca. 10 times faster than the latter [E^0 ($SiW_{12}O_{40}^{4-}/SiW_{12}O_{40}^{5-}$) = 0.054 V][5e,14] with Ag^+ ions (Figure 4), leading to smaller and less dispersed silver particles of mean diameter 6.6 ± 0.9 nm, relative to those obtained by the reaction of $SiW_{12}O_{40}^{5-}$, 29.2 ± 4.7 nm (Figure 7).

3.2. Influence of the Different Degree of Reduction of the Same POM

The reducing power of POMs is switched on by using UV irradiation. Prolonged irradiation of a (POM/propan-2-ol) solution results in accumulation of electrons on the POM (herein $P_2Mo_{18}O_{62}^{6-}$ is photoreduced to $P_2Mo_{18}O_{62}^{8-}$ and then to $P_2Mo_{18}O_{62}^{10-}$, while $P_2W_{18}O_{62}^{6-}$ is photoreduced to $P_2W_{18}O_{62}^{7-}$ and then $P_2W_{18}O_{62}^{8-}$). In this way, the redox potential shifts to more negative, yet distinct, values (Figure 2), which are decisive for the rate of reaction (2) and the selectivity of the process.

After photoreduction reaches the desired values, the resulting POM(e-)/propan-2-ol solution is moved from the photolysis lamp and a Ag^+ solution is added in the dark. Reaction (2) is not observed between the two-electron-reduced phosphomolybdate, $P_2Mo_{18}O_{62}^{8-}$, and Ag^+ ions even after 26 hours [$E^0(P_2Mo_{18}O_{62}^{6-}/P_2Mo_{18}O_{62}^{8-})$ = 0.664 V].[5e] On the contrary, when using the four-electron-reduced POM, $P_2Mo_{18}O_{62}^{10-}$, and under the same conditions, at 10^{-4} M, the formation of silver nanoparticles is completed within 200 min upon the addition of 0.5×10^{-4} M Ag^+ [$E^0(P_2Mo_{18}O_{62}^{8-}/P_2Mo_{18}O_{62}^{10-})$ = 0.514 V].[5e] The stoichiometry $[P_2Mo_{18}O_{62}^{10-}]/[Ag^0]$ = 1:2 is observed throughout the reaction, suggesting the reoxidation of $P_2Mo_{18}O_{62}^{10-}$ to $P_2Mo_{18}O_{62}^{8-}$ and its action as a two-electron donor.

In a similar way, the one-electron-reduced phosphotungstate, $P_2W_{18}O_{62}^{7-}$ [$E^0(P_2W_{18}O_{62}^{6-}/P_2W_{18}O_{62}^{7-})$ = 0.344 V][5e,15] is measured to be ca. three times slower in reducing silver than the two-electron-reduced phosphotungstate, $P_2W_{18}O_{62}^{8-}$ [$E^0(P_2W_{18}O_{62}^{7-}/P_2W_{18}O_{62}^{8-})$ = 0.144 V].[5e,15] The corresponding visible absorption spectra in Figure 8 suggest that the faster POM, that is $P_2W_{18}O_{62}^{8-}$, results in smaller silver particles than those obtained from $P_2W_{18}O_{62}^{7-}$, as indicated by the blueshift and the higher absorbance of the plasmon resonance peak of the former. In addition, less dispersed particles are formed by the faster $P_2W_{18}O_{62}^{8-}$ as derived from the more symmetrical absorption peak at 420 nm.

In view of Figure 6–8, the more negative the $E^0_{POM/POM(e-)}$ values the faster the electron transfer to Ag^+

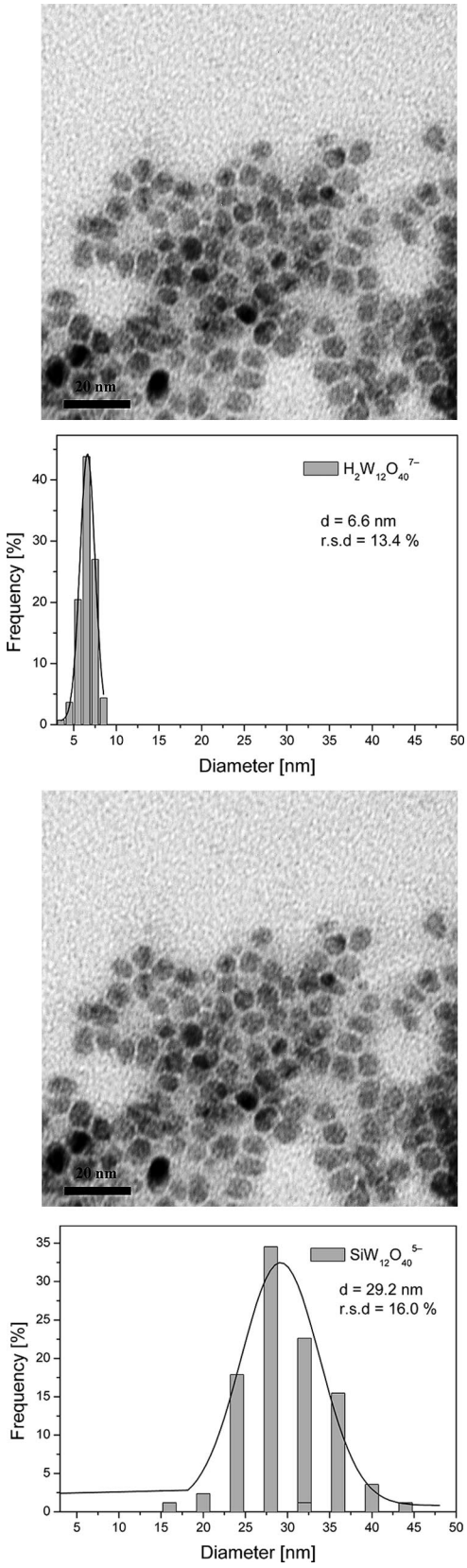

Figure 7. Transmission electron micrographs (TEM) and the corresponding size histograms of the silver particles obtained for various types of POM. Reduced POM (1.3×10^{-4} M) [obtained by illumination of a deaerated solution POM (2.0×10^{-4} M) and propan-2-ol (1.0 M)], Ag^+ (1.0×10^{-4} M).

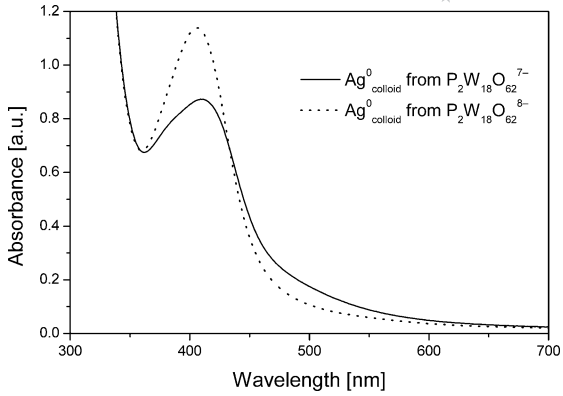

Figure 8. Influence of the extent of reduction of POM (1- or 2-equivalent-reduced $P_2W_{18}O_{62}^{6-}$) on the size of the silver nanoparticles obtained, as revealed by the corresponding absorption spectra. Results obtained by mixing reduced POM, $P_2W_{18}O_{62}^{7-}$ or $P_2W_{18}O_{62}^{8-}$ (1.0×10^{-4} M) [made by illumination of a deaerated solution POM (1.2×10^{-4} M) and propan-2-ol (2.0 M)], Ag^+ (0.8×10^{-4} M). (The $P_2W_{18}O_{62}^{6-}$ solution was prefiltered).

and the smaller the particles. Faster reductions lead to smaller nanoparticles as a result of favoring nucleation vs. growth. Dispersity is also lowered.

3.3. Comparison between POM Nanocathodes Relative to Conventional Electrodes

During the last decade, conventional electrochemistry has appeared as a practical method for the synthesis of metal nanoparticles in organic or aqueous solutions. In an elegant way, the cathode mediates the electron transfer to metal ions, producing *pure* metal products, surrounded solely by the stabilizing molecules, while size-control can be imposed by manipulating the *electron flow* through variation of operational parameters such as the current density or the current flow.[16a,16b] This, in some way, is reminiscent of the POM-based process in which the POM molecules act as electron relays for the reduction of silver ions to produce *pure* silver nanoparticles since they are stabilized by solely one kind of molecule (the POM anion that serves its dual role of reductant and stabilizer) avoiding the necessity to add a second chemical. Moreover, size-selectivity is achieved via control of the *electron flow* to Ag^+ ions, through variation of the reducing power of POM.

The electrodeposition of large metal particles on the cathode material is a facile process, which, however, leads to the coverage of the cathode surface and finally prevents the formation of the desirable nanoparticles, especially with noble metals, for instance silver. In these cases, a vigorous mechanical stirring, or sonication, is essential in order to rapidly remove the reduced metal particles from the vicinity of the cathode. In this way, the formation of nanoparticles is subject to mass-transfer limitations and becomes irreproducible. Even in an improved method, where a stabilizer is added in addition to stirring, the process remains rather irreproducible.[17] A 36% size distribution and high tailing have been observed.[18]

We show herein that using POMs as non-conventional electrodes, some of the hurdles that traditional electrochem-

ical processes exhibit are overcome: (i) POMs not only do not promote their coverage by large metal particles, but also they stabilize them in nanometer dimensions and (ii) instead of being subject to (irreproducible) mass-transfer limitations, the process remains reaction-limited even under our conditions without stirring, as depicted by the formation of silver nanoparticles which parallels the reoxidation of POM(e-) (Figure 4). This is attributed to the homogeneous nature of the process, where the POM molecular nanoelectrodes diffuse rapidly to the entire solution volume, imposing their reducing/stabilizing ability uniformly in the bulk. As a result, more uniform metal nanoparticles of narrow size distribution are obtained in the POM-based process (with relative standard deviation, r.s.d., less than 21% in any case), relative to about 36% for the traditional electrochemical methods.[18]

Moreover, POM nanocathodes could also utilize their unique redox and stabilizing ability in a multidisciplinary mode, triggered by other processes, for instance, UV/near-visible light, γ-rays,[19] or chemical reductants.[20]

4. Size Control by Changing the Concentration of Ag^+

Deaerated aqueous solutions of $SiW_{12}O_{40}^{4-}$ (1.0 mM) and propan-2-ol (1.0 M) were photolyzed and monitored at 730 nm to obtain one-electron-reduced blue $SiW_{12}O_{40}^{5-}$ (7×10^{-4} M). To these solutions were added various amounts of Ag^+, and the rate of reoxidation of $SiW_{12}O_{40}^{5-}$ was again monitored at 730 nm. It turned out that the rate of $SiW_{12}O_{40}^{5-}$ reoxidation and consequently that of silver formation, remained practically constant at ca. 8×10^{-4} M min^{-1} for $[Ag^+]_0 \geq 0.5\times10^{-4}$ M.

Thus, roughly the same number of seeds is formed during the first stages of the process, for various $[Ag^+]_0$. By increasing $[Ag^+]_0$: (i) a greater amount of silver has to be deposited on the same number of seeds and (ii) the ratio [metal]/[stabilizer] increases, and the amount of POM might not suffice for stabilization. In any case larger particles are expected. The results are shown in Table 2 and Figure S4. {See also the visible absorption spectra of the corresponding nanoparticles in the Supporting Information, Figure S5, which exhibit a redshift with increasing $[Ag^+]_0$ (Figure S6) denoting an increase in their size.[10]}

Table 2. Average size of silver nanoparticles obtained upon reduction of various Ag^+ concentrations by $SiW_{12}O_{40}^{5-}$ (ca. 7×10^{-4} M).

$[Ag^+]_0$ [M]	Diameter[a] [nm]	r.s.d.[b] [%]
5.7×10^{-4}	62.3	±17.3
2.0×10^{-4}	42.9	±17.4
1.0×10^{-4}	33.3	±20.6

[a] Average diameter based on the counting of ca. 150 particles from the corresponding TEM images (Figure S4). [b] r.s.d.: relative standard deviation.

In addition, by using even lower $[Ag^+]_0$, 0.2×10^{-4} M, even smaller silver particles are produced, as verified by: (i) their plasmon resonance peak, which is at even lower wavelengths (Figures S5 and S6) and (ii) their instability to air oxidation (they were reoxidized minutes after the opening of the reaction cell to the air, and TEM measurements could not be obtained), since, in general, smaller metal nanoparticles are more amenable to oxidations.

Figure 9 shows the variations in the color of the as-prepared solutions of silver nanoparticles from light yellow to yellow, green, and white-grey as the amount of silver was increased from 0.2 to 1.0, 2.0, and 5.7×10^{-4} M, respectively.

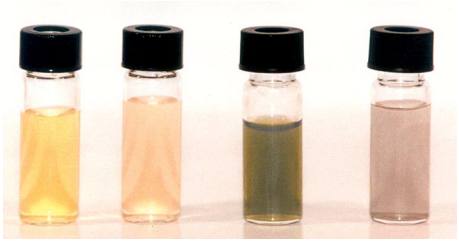

Figure 9. Photographs of the solutions of silver nanoparticles of varied concentrations of silver. From left to right, solutions of 1.0 to 0.2, 2.0, and 5.7×10^{-4} M Ag^+, respectively.

Conclusions

Uniform, size-controlled silver nanoparticles were easily obtained by simply mixing reduced POM and silver ions at room temperature.

Control of the size of the particles is achieved by changing the rate of silver reduction. Faster reductions result in smaller and more uniform spherical silver nanoparticles, as exhibited by: increasing the concentration of reduced POM, accumulating electrons on the same POM, or using POMs having more negative reduction potential. A precise redox-control on the rate of electron transfer , $\log k$ (E^0), is observed, which illustrates the "soluble cathode" behavior of POMs, which can form very uniform particles relative to the conventional electrochemical reductive methods.

Control of the size of the obtained particles was also achieved by varying the amount of silver: greater amounts of Ag^+ result in larger particles.

The ability of POMs to be reduced in a multitude of ways (photolytically, radiolytically, electrolytically, and chemically), combined with the ability of reduced POMs to transfer electrons to other metals to form various nanostructures (nanorings, sheets, rods), could extend the applications of this size-selective process.

Experimental Section

Materials: $AgNO_3$ (99%) and $H_4SiW_{12}O_{40}$ (analytical grade) were obtained from Panreac and Aldrich, respectively, and used as received. $Na_6H_2W_{12}O_{40}$, $K_6P_2W_{18}O_{62}$, and $(NH_4)_6P_2Mo_{18}O_{62}$ were made in our laboratory according to known synthetic procedures.[14] Propan-2-ol was analytical grade, while ultra pure water was obtained from a Purelab apparatus (HPLC grade). Extra pure argon (99.999%) was used to deaerate the solutions.

Preparation of Reduced POM Solutions, Reaction (1): In order to produce solutions of reduced POM, an aqueous solution of POM (4 mL, usually ca. 10^{-4} to 2×10^{-4} M) and propan-2-ol (ca. 1 M), at pH ca. 5 without adjustment, were placed into a spectrophotometer cell (1 cm path length), deaerated with Ar, and then covered with a serum cap. Photolysis was performed with a 1000 W Xe arc lamp at which the light intensity was reduced mechanically by ca. 40%, while cut-off filters at 320 nm were used to avoid direct photolysis of organic substrates. Upon illumination, the solution turned blue due to the formation of reduced POM, POM(e-), by reaction (1). The illumination time was adjusted (varied in minutes timescale, depending on the POM and the concentrations) in order to obtain the desired concentration of reduced POM, precisely measured in each case by UV/Vis absorption spectrometry. Higher illumination times resulted in higher concentrations of reduced POM, while prolonged illumination led to the formation of extensively reduced POMs (two-electron-reduced for $P_2W_{18}O_{62}^{6-}$ and four-electron-reduced for $P_2Mo_{18}O_{62}^{6-}$).

Synthesis of Silver Nanoparticles, Reaction (2): In turn, in the absence of light, silver nanoparticles were obtained by injecting a deaerated aqueous solution of $AgNO_3$ (the necessary volume of a 3.83×10^{-3} M or 0.0115 M solution was added in order to obtain a concentration of silver ions of ca. 10^{-4} M) to the already prepared POM(e-) solution (4 mL), which remained sealed with the serum cap. The solutions were mixed, agitated for ca 3 s and allowed to stand. The initially blue solution turned green and finally yellow within a time period between seconds and hours depending on the POM used.

Monitoring of Reaction (2)

Analysis of POM(e-) and Silver Nanoparticles: The analysis of the reduced POM was executed with a UV/Vis absorption spectrometer, a Perkin–Elmer Lambda 19 Spectrometer, by monitoring the characteristic absorbance of the blue POM(e-) species [$SiW_{12}O_{40}^{5-}$ ε_{730nm} = 2100 $M^{-1}cm^{-1}$; $H_2W_{12}O_{40}^{7-}$ ε_{690nm} = 2100 $M^{-1}cm^{-1}$; $P_2W_{18}O_{62}^{7-}$ ε_{714nm} = 3600 $M^{-1}cm^{-1}$; $P_2W_{18}O_{62}^{8-}$ ε_{694nm} = 10600 $M^{-1}cm^{-1}$; $P_2Mo_{18}O_{62}^{8-}$ ε_{756nm} = 11000 $M^{-1}cm^{-1}$; $P_2Mo_{18}O_{62}^{10-}$ ε_{675nm} = 19400 $M^{-1}cm^{-1}$].[21] The concentration of Ag^0 nanoparticles was measured from the increase in the absorbance at ca. 420 nm, attributed to the plasmon resonance peak of colloidal silver, taking as absorption coefficient the one calculated at the saturation point of the reaction when all silver had been reduced.

Characterization of Silver Nanostructures: The silver nanoparticles obtained were characterized by transmission electron microscopy. TEM images were obtained with a Philips 200 kV microscope, while the samples were prepared by placing microdrops of colloid solution on a Formvar/Carbon coated copper grid. The subsequent analysis for the size distribution of the particles was based on the counting of ca. 150 particles.

Calculation of the Initial Rate Values: The initial rate of POM(e-) reoxidation was calculated by the slope of the curve of the concentration of POM(e-) vs. time of the reaction with silver ions, for conversions less than 30%.

Supporting Information (see footnote on the first page of this article): Figures showing the TEM images and size histograms as well as the variations of UV/Vis spectra, the shift in the plasmon resonance absorbance by increasing the initial concentration of either reduced POM $SiW_{12}O_{40}^{5-}$ (Figures S1–S3) or silver ions (Figures S4–S6).

Acknowledgments

A. T. and T. T are grateful to the National Centre for Scientific Research (NCSR) "Demokritos", Institute of Physical Chemistry, for post-doctoral fellowships. We are grateful to Dr. A. Travlos for his significant contribution with the TEM measurements.

[1] a) K. Kim, I. Lee, S. J. Lee, *Chem. Phys. Lett.* **2003**, *377*, 201–204; b) P. V. Kamat, *J. Phys. Chem. B* **2002**, *106*, 7729–7744; c) V. Subramanian, E. E. Wolf, P. V. Kamat, *Langmuir* **2003**, *19*, 469–474; d) A. Henglein, *Ber. Bunsenges. Phys. Chem.* **1995**, *99*, 903–913; e) J. Kiwi, M. Grätzel, *J. Am. Chem. Soc.* **1979**, *101*, 7214–7217.

[2] a) R. Schlögl, S. B. A. Hamid, *Angew. Chem. Int. Ed.* **2004**, *43*, 1628–1637; b) M.-C. Daniel, D. Astruc, *Chem. Rev.* **2004**, *104*, 293–346; c) L. M. Liz-Marzán, P. V. Kamat in *Nanoscale Materials* (Eds.: L. M. Liz-Marzán, P. V. Kamat), Kluwer Academic Publishers, Boston/Dordrecht/London, **2003**; d) J. A. Widegren, R. G. Finke, *J. Mol. Catal. A* **2003**, *198*, 317–341; e) A. Roucoux, J. Schulz, H. Patin, *Chem. Rev.* **2002**, *102*, 3757–3778; f) B. J. Hornstein, J. D. Aiken III, R. G. Finke, *Inorg. Chem.* **2002**, *41*, 1625–1638; g) J. D. Aiken III, R. G. Finke, *J. Mol. Catal. A* **1999**, *145*, 1–44; h) J. D. Aiken III, R. G. Finke, *J. Am. Chem. Soc.* **1999**, *121*, 8803–8810; i) J. Y. Ying, T. Sun, *J. Electroceram.* **1997**, *1:3*, 219–238; j) G. Schmid in *Clusters And Colloids: From Theory To Applications* (Ed.: G. Schmid), VCH Publishers, New York, **1994**; k) A. Henglein, *J. Phys. Chem.* **1993**, *97*, 5457–5471; l) L. N. Lewis, *Chem. Rev.* **1993**, *93*, 2693–2730.

[3] a) Y. Song, Y. Yang, C. J. Medforth, E. Pereira, A. K. Singh, H. Xu, Y. Jiang, C. J. Brinker, F. Swol, J. A. Shelnutt, *J. Am. Chem. Soc.* **2004**, *126*, 635–645; b) Z. S. Pillai, P. V. Kamat, *J. Phys. Chem. B* **2004**, *108*, 945–951; c) D. D. Evanoff Jr, G. Chumanov, *J. Phys. Chem. B* **2004**, *108*, 13948–13956; d) H. Bönnemann, R. M. Richards, *Eur. J. Inorg. Chem.* **2001**, 2455–2480; e) K. Okitsu, A. Yue, S. Tanabe, H. Matsumoto, H. Yobiko, *Langmuir* **2001**, *17*, 7717–7720; f) M. T. Reetz, M. Maase, *Adv. Mater.* **1999**, *11*, 773–777; g) T. Teranishi, M. Miyake, *Chem. Mater.* **1998**, *10*, 594–600; h) T. Teranishi, I. Kiyokawa, M. Miyake, *Adv. Mater.* **1998**, *10*, 596–599; i) D. V. Goia, E. Matijević, *New J. Chem.* **1998**, *22*, 1203–1215; j) M. A. Watzky, R. G. Finke, *Chem. Mater.* **1997**, *9*, 3083–3095; k) H. H. Huang, X. P. Ni, G. L. Loy, C. H. Chew, K. L. Tan, F. C. Loh, J. F. Deng, G. Q. Xu, *Langmuir* **1996**, *12*, 909–912; l) J. Turchevich, G. Kim, *Science* **1970**, *169*, 873–879.

[4] A. Troupis, A. Hiskia, E. Papaconstantinou, *Angew. Chem. Int. Ed.* **2002**, *41*, 1911–1914.

[5] a) E. Papaconstantinou, A Hiskia, in *Polyoxometalate Molecular Science* (Eds.: J. J. Borrás-Almenar, E. Coronado, A. Müller M. Pope), Kluwer Academic Publishers: The Netherlands, **2003**, p. 381–416; b) T. Yamase, *Catal. Surv. Asia* **2003**, *7*, 203; c) A. Hiskia, A. Mylonas, E. Papaconstantinou, *Chem. Soc. Rev.* **2001**, *30*, 62–69; d) C. L. Hill, C. M. Prosser-McCarthain in *Photosensitization and Photocatalysis Using Inorganic and Organometallic Compounds* (Eds.: K. Kalyanasundaram, M. Grätzel), Kluwer Academic Publishers, The Netherlands, **1993**, p. 307; e) E. Papaconstantinou, *Chem. Soc. Rev.* **1989**, *18*, 1–31; f) M. S. Rindl, *Afr. J. Sci.* **1916**, *11*, 362–366.

[6] a) M. Sastry, A. Swami, S. Mandal, Pr. Selvakannan, *J. Mat. Chem.* **2005**, *15*, 3161–3174; b) S. Mandal, P. R. Selvakannan, R. Pasricha, M. Sastry, *J. Am. Chem. Soc.* **2003**, *125*, 8440–8441; c) A. Sanyal, M. Sastry, *Chem. Commun.* **2003**, *11*, 1236–1237; d) S. Mandal, D. Rautaray, M. Sastry, *J Mater. Chem.* **2003**, *13*, 3002–3005.

[7] a) A. V. Gordeev, N. I. Kartashev, B. G. Ershov, *High Energy Chem.* **2002**, *36*, 102–106; b) B. G. Ershov, A. V. Gordeev, *Mendeleev Commun.* **2001**, 147–148; c) A. V. Gordeev, B. G. Ershov, *High Energy Chem.* **1999**, *33*, 218–223.

[8] a) L. Yang, Y. Shen, A. Xie, J. Liang, S. Li, Q. Zhang, *Eur. J. Inorg. Chem.* **2006**, 4658–4664; b) A. Hiskia, E. Papaconstantinou, A. Troupis, *International Patent* PCT/GR 2004/oo49, WO2006/038045 A1, **2006**.

[9] Following the comments of a referee, we note that contrary to $PW_{12}O_{40}^{4-}$, further oxidation of $SiW_{12}O_{40}^{5-}$ and $H_2W_{12}O_{40}^{7-}$ is noticed after complete reduction of Ag^+ to Ag^0. This might be attributed to the more negative potentials of $SiW_{12}O_{40}^{5-}$ and $H_2W_{12}O_{40}^{7-}$ (Figure 2) capable of causing further reduction of silver nanoparticles; (see for instance: a) T. Hirakawa P. V. Kamat, *Langmuir* **2004**, *20*, 5645–5647; b) V. Subramanian, E. E. Wolf, P. V. Kamat, *J. Am. Chem. Soc.* **2004**, *126*, 4943–4950). In support of this is that $SiW_{12}O_{40}^{5-}$ with less negative potential than $H_2W_{12}O_{40}^{7-}$ (Figure 2) undergoes partial reoxidation, whereas, reoxidation of $H_2W_{12}O_{40}^{7-}$ seems to go to completion (Figure 4b, c).

[10] S. M. Heard, F. Grieser, C. G. Barraclough, *J. Colloid Interface Sci.* **1983**, *93*, 545–555.

[11] Y. Lin, R. G. Finke, *J. Am. Chem. Soc.* **1994**, *116*, 8335–8353.

[12] L. Eberson, L.-G. Wistrand, *Acta Chem. Scand. B* **1980**, *34*, 349–357.

[13] k is the rate constant of reaction (2) in min^{-1}. Since reaction (2) is first order in POM(e-) and zeroth order in Ag^+, k is derived by dividing the initial rate of POM(e-) reoxidation, measured by the lowering of the characteristic absorbance of the blue POM(e-) at ca. 730 nm, by the initial concentration of POM(e-). Typical data for thermal (dark)reaction (2) for $SiW_{12}O_{40}^{5-}$, from which the data of (Figure 6) are calculated, are shown on (Figure 5).

[14] M. T. Pope, G. M. Varga, *Inorg. Chem.* **1966**, *5*, 1249–1254.

[15] M. T. Pope, E. Papaconstantinou, *Inorg. Chem.* **1967**, *6*, 1147–1152.

[16] a) M. T. Reetz, M. Winter, R. Breinbauer, T. Thurn-Albrecht, W. Vogel, *Chem. Eur. J.* **2001**, *7*, 1084–1094; b) M. T. Reetz, W. Helbig, *J. Am. Chem. Soc.* **1994**, *116*, 7401–7402.

[17] Y. Socol, O. Abramson, A. Gedanken, Y. Meshorer, L. Berenstein, A. Zaban, *Langmuir* **2002**, *18*, 4736–4740.

[18] B. Yin, H. Ma, S. Wang, S. Chen, *J. Phys. Chem. B* **2003**, *107*, 8898–8904.

[19] E. Papaconstantinou, *J. Chem. Soc. Faraday Trans. 1* **1982**, *78*, 2769–2772.

[20] I. A. Weinstock, *Chem. Rev.* **1998**, *98*, 113–170.

[21] a) G. M. Varga Jr, E. Papaconstantinou, M. T. Pope, *Inorg. Chem.* **1970**, *9*, 662–667; b) E. Papaconstantinou, M. T. Pope, *Inorg. Chem.* **1970**, *9*, 667–669.

Received: August 12, 2008
Published Online: November 10, 2008

